

# SCIENTIFIC REPORTS



OPEN

## Ultralong well-aligned $\text{TiO}_2:\text{Ln}^{3+}$ (Ln = Eu, Sm, or Er) fibres prepared by modified electrospinning and their temperature-dependent luminescence

Received: 24 November 2016

Accepted: 01 February 2017

Published: 07 March 2017

Hongquan Yu<sup>1</sup>, Yue Li<sup>1</sup>, Yang Song<sup>1</sup>, Yanbo Wu<sup>1</sup>, Xijie Lan<sup>1</sup>, Shimin Liu<sup>1</sup>, Yanning Tang<sup>1</sup>, Shasha Xu<sup>1</sup> & Baojiu Chen<sup>2</sup>

Electrospinning has emerged as an attractive technique for the fabrication of ultrafine fibres in micro-/nano-scale fineness; however, it remains a significant technological challenge to assemble aligned fibre arrays via an conventional electrospinning method due to the inherent whipping instability of the polymeric jet. We herein have first developed a simple modified electrospinning method with which to prepare ultralong (>300 mm) well-aligned inorganic fibre arrays, *i.e.*, using an ultrahigh molecular weight polymer to suppress or eliminate the whipping motion of the electrospun jet, has emerged as a facile approach for the continuous fabrication of well-aligned, ultralong fibres through simply using a rotating cylinder as the collector (it was not found necessary to use a very high rotating speed, extra magnetic, electrical field) in the electrospinning process. As result, the ultralong well-aligned  $\text{TiO}_2:\text{Ln}^{3+}$  (Ln = Eu, Sm, or Er) fibre arrays can be obtained from ultrahigh molecular weight poly(ethylene oxide), tetra-*n*-butyl titanate ( $\text{Ti}(\text{OC}_4\text{H}_9)_4$ ) and lanthanide nitrate in the modified electrospinning approach. The grow mechanism and luminescent properties of these ultralong well-aligned  $\text{TiO}_2:\text{Ln}^{3+}$  fibre arrays were also investigated.

In past twenty years, one-dimension (1-d) titania nanostructures have attracted rapidly increasing attention due to their important role in applications related to gas sensing, optoelectronic devices, biomedicine, in the fabrication of solar cells and batteries<sup>1–9</sup>. However, disordered structures are problematic for use in device fabrication in such areas as microelectronics, photonics. Therefore, researchers has explored novel methods including the hydrothermal route, the AAO template method, the electrochemical approach etc. to improve the alignment of 1-d titania nanostructures in past decades<sup>10–12</sup>. However, the yield production of the 1-d titanium arrays obtained from these methods is much less, not in sufficient quantities to satisfy commercial demand. And these titanium arrays in length have just several hundred microns. It is known that, the electrospinning technique is an effective way to produce polymer or inorganic fibres with diameters as small as 10 nm and up to a few microns in diameter. This approach is inexpensive, easily operated, non-polluting, and available suits for industrial production. The length of the nanofibres depends on the time of electrospinning and can be thousands of kilometres (in theory)<sup>13</sup>. However, under normal conditions, bending instabilities of polymer jet are the primary cause of generate randomly oriented fibres with various diameters and structures during the electrospinning process<sup>14,15</sup>. In past decades, researchers has explored novel methods including mechanical, electrostatic, and other ways of improving the alignment of electrospun nanofibres<sup>16–18</sup>. These methods comprising largely of using high speed collectors and/or through manipulating the electrical field have been devised and shown to work well in preparing aligned electrospun fibres and patterns. However, the set-up used is somewhat complicated or the alignment of as-spun fibres cannot be maintained with increasing collection time due to the varying electrical conductivity of the

<sup>1</sup>College of Environmental and Chemical Engineering, Dalian Jiaotong University, Dalian, Liaoning 116028, P. R. China.

<sup>2</sup>Department of Physics, Dalian Maritime University, Dalian, Liaoning 116026, P. R. China. Correspondence and requests for materials should be addressed to H.Y. (email: yuhq7808@djtu.edu.cn) or B.C. (email: bjchen@dmlu.edu.cn)

collector caused by increased numbers of fibre layers. Therefore, it remains a significant technological challenge to assemble aligned fibre arrays via an conventional electrospinning method.

Recent years, the nanoscale lanthanide doped compounds in particular 1-d nanostructures have attracted much research interest for their broad potential applications-e.g. color display, solar cells, ultrasensitive detection and *in vivo* imaging<sup>19–23</sup>. Thus, developing an strategy to easily obtain mass-scale manufacturing of the 1-d lanthanide doped nanostructures is very significant to satisfy practical applications. In the present work, we develop a improved the conventional electrospinning technique to large-scale easily produce ultralong parallel well-aligned  $\text{TiO}_2\text{:Ln}^{3+}$  ( $\text{Ln} = \text{Sm}, \text{Eu}, \text{or Er}$ ) fibre arrays. In this method, the ultrahigh molecular weight PEO was exploited to eliminate the occurrence bending instability of the electrospinning jet to achieving highly aligned fibre assemblies. In addition, the grow mechanism and luminescence properties of well-aligned  $\text{TiO}_2\text{:Ln}^{3+}$  fibre arrays were also investigated. This simple approach can achieve ultra-long aligned inorganic nanofibres and nanostructures arrays in a straightforward and scalable fashion, suitable for a variety of practical applications.

## Experimental Procedure

Some 2.0 g of tetra-*n*-butyl titanate ( $\text{Ti}(\text{OC}_4\text{H}_9)_4$ ) was dropped in the mixed solvent with 5 ml of ethanol and 15 ml of  $\text{CH}_2\text{Cl}_2$  under magnetic stirring for 20 min. Then a certain amount of rare earth nitrate such as  $\text{Eu}(\text{NO}_3)_3$ ,  $\text{Sm}(\text{NO}_3)_3 \cdot 6\text{H}_2\text{O}$ , or  $\text{Er}(\text{NO}_3)_3 \cdot 6\text{H}_2\text{O}$  was added to this mixture, respectively. The molar ratio of  $\text{Eu}^{3+}$  to  $\text{Ti}^{4+}$  was 1.0, 3.0, 5.0, and 10.0 mol %, respectively. The molar ratio of  $\text{Sm}^{3+}$  to  $\text{Ti}^{4+}$  was 1.0, 5.0 and 10.0 mol%, respectively. The molar ratio of  $\text{Er}^{3+}$  to  $\text{Ti}^{4+}$  was 1.0 mol%. After 20 min, an amount of PEO was added to the aforementioned mix solution, followed by magnetic stirring for about 1 h to obtain the final electrospinning solution. Supplementary Figure 1 shows the schematic diagram of the electrospinning set-up, which consisted of three major parts: a high-voltage power supply, a spinneret (plastic needle), and a collector (rotating plastic drum). The precursors of  $\text{TiO}_2\text{:Ln}^{3+}$  ( $\text{Ln} = \text{Sm}, \text{Eu}, \text{or Er}$ ) fibre arrays were obtained by electrospinning with a distance of 200 mm between the spinneret tip and the collector, an applied voltage of 5.0 to 8.0 kV at a rate of rotation of the drum of between 500 to 1400 rpm (1 rpm was equivalent to a linear speed of 0.0067 m/s). The as-prepared precursor fibres of the  $\text{TiO}_2\text{:Ln}^{3+}$  array were taken off and calcined at a heating rate of  $10^\circ\text{C} \cdot \text{h}^{-1}$  in air to remove organic components, thus forming ceramic  $\text{TiO}_2 \text{Ln}^{3+}$  fibres.

The crystal structure of the samples was studied by powder X-ray diffractometer (XRD, Shimadzu, XRD-6000) with  $\text{Cu K}\alpha$  radiation ( $\lambda = 0.15406 \text{ nm}$ ). In the X-ray diffraction measurements, the scanning region was  $20^\circ \leq 2\theta \leq 80^\circ$ , and the scanning step size was  $0.02^\circ$ . The morphology of the samples was observed by field emission scanning electron microscope (SEM, SUPRA 55). The TEM images, HR-TEM images, and selected area electron diffraction patterns (SAED) of the HR-TEM images were recorded on a JSM-2010 transmission electron microscope (JEM, Japan) under a working voltage of 200 kV. The excitation and emission spectra were recorded on a Hitachi F-4600 spectrophotometer equipped with a continuous 150 W Xe arc lamp: for comparison between different samples, the emission spectra were measured at a fixed pass of 0.2 nm with the same instrument parameters (a 2.5 nm excitation split, a 2.5 nm emission split, and a 400 V photomultiplier tube voltage).

## Results and Discussion

Changing the electrospinning conditions, such as the applied voltage, the PEO content, and the rate of rotation of the collecting drum, all exerted a significant influence on the size and morphology of the precursor fibres of  $\text{TiO}_2$ . Supplementary Figures 2 to 5 show the FE-SEM images of the  $\text{TiO}_2$  precursors fibres prepared under different conditions. Accordingly, it can be found that the obtained  $\text{TiO}_2$  precursor fibres have random structures with regards their spatial orientation when the rate of rotation of the collecting drum was less than the 800 rpm, while aligned  $\text{TiO}_2$  fibres were obtained when the rate of rotation of the drum exceeded 1100 rpm. The orientation of the as-spun fibres was improved with increasing rate of rotation of the collecting drum. Besides, Supplementary Fig. 2(e) and (f) further confirm that the precursor  $\text{TiO}_2$  fibres are well-aligned fibre arrays. Within the range studied, an increased PEO and  $\text{Ti}(\text{OC}_4\text{H}_9)_4$  concentration caused the diameter of the precursor fibres to increase gradually. The PEO concentration was 1.0, 2.0, 2.5, and 3.0 wt%, the corresponding average diameters of the  $\text{TiO}_2$  precursors fibres were 3.0  $\mu\text{m}$ , 4.2  $\mu\text{m}$ , 5.0  $\mu\text{m}$ , and 6.0  $\mu\text{m}$ , while the  $\text{Ti}(\text{OC}_4\text{H}_9)_4$  concentration was 8.0, 10.0, or 20.0 wt%, the corresponding average diameters of the  $\text{TiO}_2$  precursors fibres are 3.5  $\mu\text{m}$ , 5.0  $\mu\text{m}$ , and 15.0  $\mu\text{m}$ , respectively. Varying the applied voltage exerted no obvious influence on the diameter of fibres, but the orientation of the as-prepared fibres proved to be dependent on the electrospinning voltage. When the applied voltage was too small ( $<5 \text{ kV}$ ), the spinning of the jet from the spinneret became more difficult due to the viscoelasticity of the electrospun solution: as the applied voltage increased ( $>10 \text{ kV}$ ), the orientation of fibres became increasingly random due to bending instability of the electrospun jet. Most importantly, it was observed that, when a little rare earth nitrate (such that the molar ratio of  $\text{RE}^{3+}$  to  $\text{Ti}^{4+}$  was less than 10.0 mol%) was added to the above electrospun solutions, which barely caused any variation in the morphology of the precursor fibres of  $\text{TiO}_2$  under the same experimental conditions.

To obtain well-aligned fibre arrays of pure  $\text{TiO}_2\text{:Ln}^{3+}$ , we submit the as-prepared aligned precursor electrospun fibres to an annealing treatment. After being annealed, the PEO content was removed from the precursor fibres and inorganic  $\text{TiO}_2\text{:Ln}^{3+}$  fibre arrays were formed. Supplementary Fig. 6 shows the XRD patterns of the aligned  $\text{TiO}_2\text{:Ln}^{3+}$  fibre array after annealing. It can be seen that the anatase phase of  $\text{TiO}_2$  was formed after calcining at between 500 and 600  $^\circ\text{C}$ . The diffraction peaks at  $2\theta$  values of  $25.3^\circ$ ,  $37.8^\circ$ ,  $48.1^\circ$ ,  $54^\circ$ ,  $62.8^\circ$ ,  $68.8^\circ$ , and  $75.1^\circ$  belong to the diffraction of the (101), (004), (200), (105), (204), (116), and (215) crystal faces of anatase  $\text{TiO}_2$  (JCPDS card no. 89–4921). With increased calcining temperature, the phase transformation from anatase into rutile  $\text{TiO}_2$  occurred. The diffraction peaks at  $2\theta$  values of  $27.5^\circ$ ,  $35.7^\circ$ ,  $41.1^\circ$ ,  $45^\circ$ ,  $54.7^\circ$ ,  $57.8^\circ$ ,  $65.4^\circ$ , and  $69.8^\circ$  came from diffraction of the (110), (101), (111), (210), (211), (220), (310), and (301) crystal faces of rutile  $\text{TiO}_2$  (JCPDS card no. 89–4920). When the calcining temperature was greater than 800  $^\circ\text{C}$ , the diffraction peaks

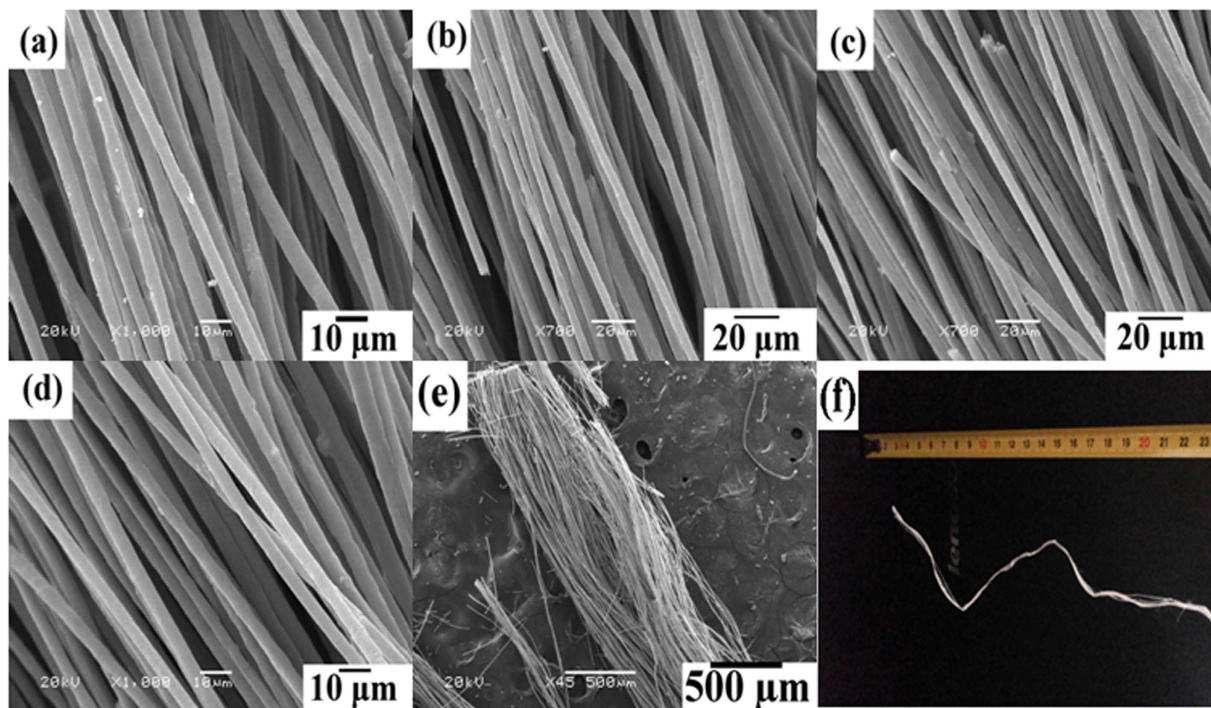


**Figure 1.** (a,b,c and d) are SEM images of well-aligned  $\text{TiO}_2:\text{Eu}$  fibre arrays from the 1.0 mol%, 3.0 mol %, 5.0 mol%, and 10.0 mol % of the  $\text{Eu}^{3+}$  concentration, respectively. (e) and (f) show an SEM image and photograph of large-scale well-aligned  $\text{TiO}_2:1.0\text{ mol\% Eu}$  fibre arrays, respectively. The concentration of PEO of was fixed at 2.5 wt %. The applied voltage was 8.0 kV and the collection distance was 20 mm. The rate of rotation of the collection drum was 1400 rpm. 1 rpm was equivalent to a linear speed of 0.0067 m/s. The as-prepared well-aligned fibres were taken off and calcined at a heating rate of  $10^\circ\text{C}\cdot\text{h}^{-1}$  and kept at  $500^\circ\text{C}$  in air for 4 h.

of anatase  $\text{TiO}_2$  disappeared and all diffraction peaks were assigned to the rutile  $\text{TiO}_2$ . In all XRD patterns, no additional  $\text{Eu}^{3+}$ ,  $\text{Sm}^{3+}$ , or and  $\text{Er}^{3+}$  diffraction peaks were observed. These results indicate that the RE ions are embedded within the  $\text{TiO}_2$  lattice.

Figure 1(a) to (f) show SEM images of well-aligned pure  $\text{TiO}_2:\text{Eu}^{3+}$  fibre arrays obtained by calcining at  $500^\circ\text{C}$ . From these images, it can be seen that the morphologies of the ceramic nanofibres were uniform. The average diameters of the single fibre were estimated to be 1.5–2.0  $\mu\text{m}$  for all samples. With increasing rare earth ion dopant concentration, their average diameters were almost unchanged. The large-scale SEM and photograph further confirm the fact that the  $\text{TiO}_2:\text{Eu}^{3+}$  fibres exhibit a well-aligned orientation and were ultralong. After annealing at  $800^\circ\text{C}$ , these  $\text{TiO}_2:\text{Eu}^{3+}$  fibres remained continuous and aligned. The TEM image of a single  $\text{TiO}_2:1\text{ mol\% Eu}^{3+}$  fibre displayed in Fig. 2: the diameter of fibre is about 1.5  $\mu\text{m}$ , and it is composed of well-aligned  $\text{TiO}_2:\text{Eu}$  nanowires of approximately 50 nm in diameter. Figure 2(c) shows the HR-TEM image of a single rutile  $\text{TiO}_2:\text{Eu}$  nanowire from the fibre. The crystal lattice fringe with a spacing  $d$  of approximately 325 nm can be observed directly, which corresponds to the (110) crystal face of rutile  $\text{TiO}_2$ , which is consistent with the XRD data. The selected area electron diffraction pattern (SEAD) of the corresponding microbelt is illustrated in Fig. 2(d) which shows the polycrystalline rings which can be indexed against rutile  $\text{TiO}_2$ . Figure 2(e) shows the scanning TEM (STEM) and corresponding energy dispersive X-ray spectroscopy (EDX) elemental mapping images, which confirmed that Ti, O, and Eu were distributed on the  $\text{TiO}_2$  fibre surface, consistent with the EDX spectrum (Supplementary Fig. 7). A very similar morphology and size were also observed from pure  $\text{TiO}_2:\text{Sm}^{3+}$  and  $\text{TiO}_2:\text{Er}^{3+}$  fibre arrays (Supplementary Figs 8 and 9). The morphology and size of the single fibre were without significant changes with increasing  $\text{Ln}^{3+}$  dopant concentrations (less than 10% molar concentrations).

It is known that, for such an electrospinning solution, the molecular weight of the polymer has a significant effect on the rheological and electrical properties, such as viscosity, surface tension, and conductivity. This is one of the most important solution parameters affecting the morphology of an electrospun fibre. Therefore, it is very difficult to prepare aligned fibres from low molecular weight PVA, PVP, PMMA, PS, and PEO when working without a high-speed rotating drum (approximately 2000 rpm), auxiliary conductors, and an external magnetic or electric field<sup>24–28</sup>. In previous reports, the PVP was used as a structure-directing template and would result in a random orientation of electrospun  $\text{TiO}_2:\text{Ln}^{3+}$  fibres and the single fibres consisted of the tight connection of multiple irregular  $\text{TiO}_2:\text{Ln}^{3+}$  nanoparticles<sup>29</sup>. In the present work, we exploited the viscoelasticity contributed by chain entanglement of the ultrahigh molecular weight PEO to eliminate the occurrence of bending instability of the electrospinning jet to achieving highly aligned fibre assemblies. And the PEO as the structure-directing template was used to obtain  $\text{TiO}_2:\text{Ln}^{3+}$  nanorods arrays in single  $\text{TiO}_2:\text{Ln}^{3+}$  fibres. A possible mechanism for the formation of well-aligned  $\text{TiO}_2:\text{Ln}^{3+}$  fibre arrays, is shown in Supplementary Fig. 8. First, the amorphous  $\text{TiO}_2$  sheaths formed at the surface of precursor fibres due to hydrolysis of  $\text{Ti}(\text{OC}_4\text{H}_9)_4$  in air during the electrospinning

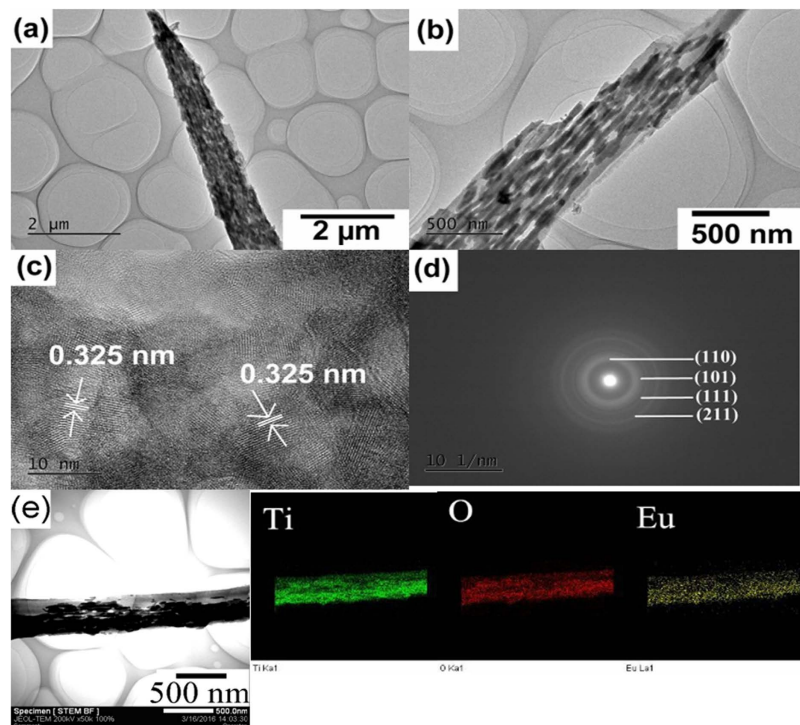


**Figure 2.** (a,b and c) are lower magnification, image of the end, and HR-TEM images of a single pure  $\text{TiO}_2\text{:Eu}$  fibre; (d) is an SAED pattern of the single pure  $\text{TiO}_2\text{:Eu}$  1.0 mol % Eu fibre. (e) STEM images and EDX elemental mapping of Ti, O and Eu of  $\text{TiO}_2\text{:Eu}$  fibre. The as-prepared well-aligned fibres were taken off and calcined at a heating rate of  $10^\circ\text{C}\cdot\text{h}^{-1}$  and kept at  $800^\circ\text{C}$  in air for 4 h.

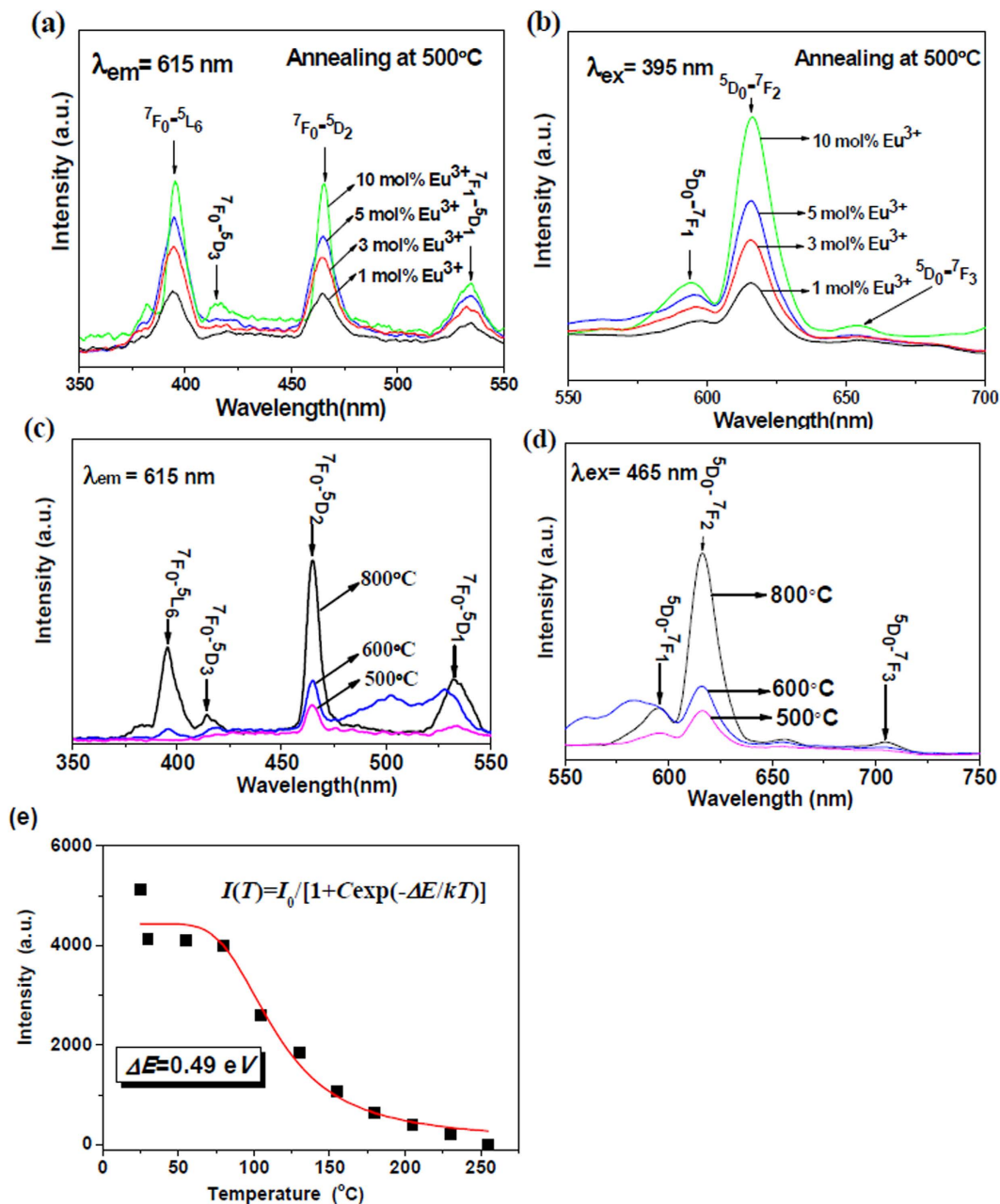
process (Supplementary Fig. 8(a)). Then, as-spun precursor fibres were annealed. Many ultrafine crystallites were combined into small nanocrystallites through mass transport and the PEO tended to be solidified with increasing temperature (Supplementary Fig. 8(b)). Finally, many small nanocrystallites were further connected to generate  $\text{TiO}_2$  nanorods due to the restriction of PEO rather than through contact points among these small different nanocrystallites to form a randomly oriented structure (Supplementary Fig. 8(c)).

Figure 3(a) to (d) show the excitation and emission spectra of well-aligned  $\text{TiO}_2\text{:Eu}^{3+}$  fibres. In the excitation spectra, the band at 200 to 280 nm was assigned to the charge transfer (CT) transition of  $\text{Eu}^{3+} \rightarrow \text{O}^{2-}$ . The CT band corresponds to the electronic transition from the  $2p$  orbital of  $\text{O}^{2-}$  to the  $4f$  orbital of  $\text{Eu}^{3+}$ , and is closely related to the covalency between  $\text{O}^{2-}$  and  $\text{Eu}^{3+}$  and the coordination environment around the  $\text{Eu}^{3+}$ . In the emission spectra, three peaks at 592 nm, 616 nm, and 656 nm were observed, which correspond to  ${}^5\text{D}_0 \rightarrow {}^7\text{F}_1$ ,  ${}^5\text{D}_0 \rightarrow {}^7\text{F}_2$ , and  ${}^5\text{D}_0 \rightarrow {}^7\text{F}_3$  transitions. As seen from the characteristic peak at 616 nm, the emission intensity increased with increasing  $\text{Eu}^{3+}$  concentration, thus implying that  $\text{Eu}^{3+}$  was not quenched while its concentration was less than 10 mol %, and agreeing with published experimental results<sup>30,31</sup>. The PL intensity of the sample increased gradually with increased calcination temperature (from 500 to  $800^\circ\text{C}$ ). The temperature-dependence of the emission intensity of  $\text{Eu}^{3+}$  at 616 nm, is shown in Fig. 3(e). It can be seen that the luminescence intensity decreased with increasing sample temperature, thus indicating temperature quenching occurred. This temperature quenching behaviour can be observed in most luminescent materials, but the quenching mechanisms are usually different. The increased temperature may result in an increase in the non-radiative relaxation rate for both cascade multiphonon transition and the energy transfer originating from the luminescent level<sup>32</sup>. In addition, the crossover process, which quenches the luminescence intensity, may occur when the temperature reaches a certain value. Usually, the fluorescence temperature quenching of  $\text{Eu}^{3+}$  doped materials follows crossover model in which the temperature dependence of fluorescence intensity can be expressed as follows<sup>33,34</sup>,

$$I(T) = \frac{I_0}{1 + C e^{-\Delta E/kT}} \quad (1)$$

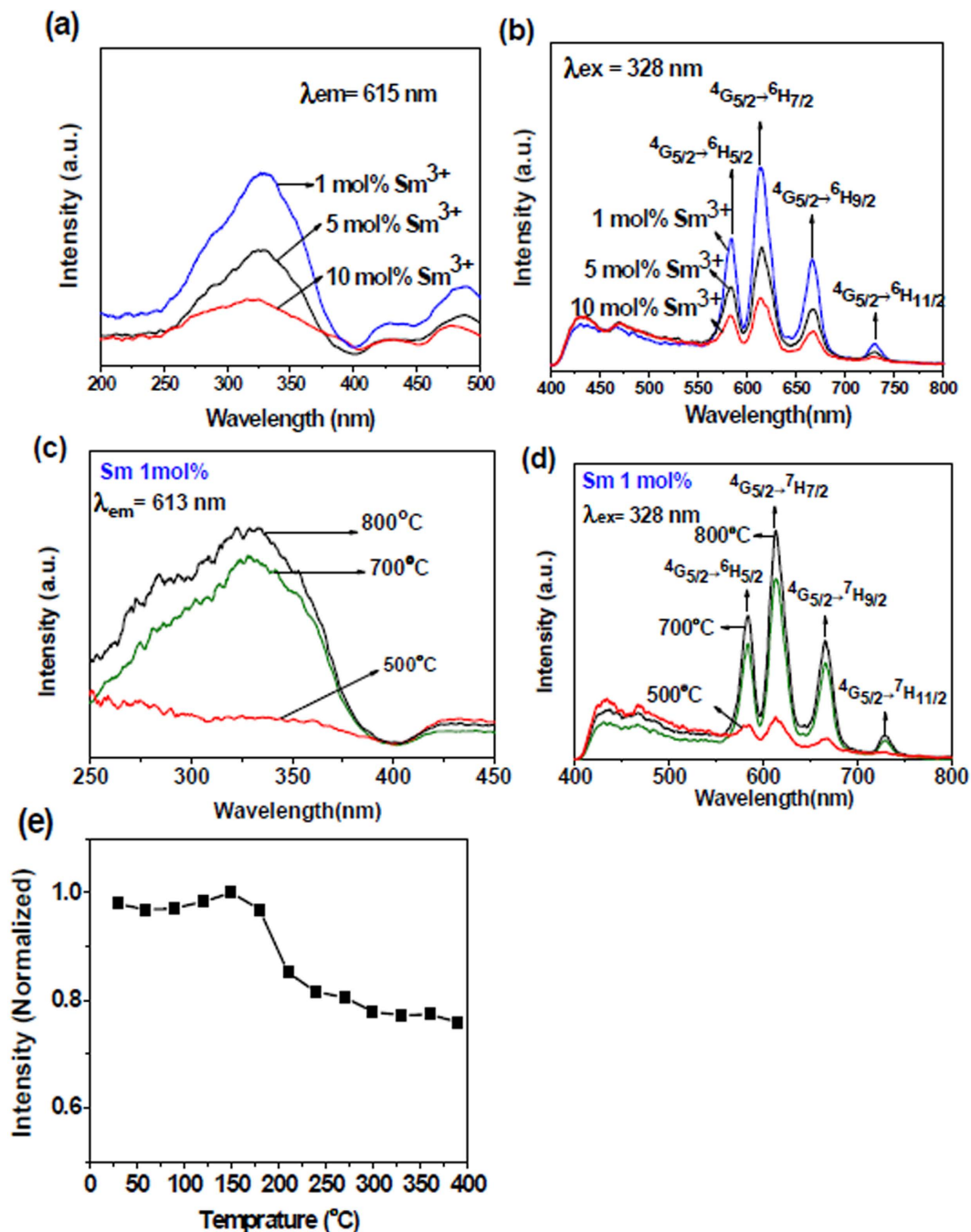
where  $I(T)$  presents fluorescence intensity at temperature  $T$ ;  $I_0$  is the initial intensity at temperature closed to  $0\text{K}$ ;  $\Delta E$  stands for the activation energy;  $k$  is Boltzmann's constant;  $C$  is a constant for a certain system. To examine the temperature quenching mechanism of  $\text{Eu}^{3+}$  fluorescence, Eq. (1) was fit to the data in Fig. 3(e), and it can be seen Eq. (1) can fit well with the data. In the fitting process, the  $\Delta E$  was confirmed to be  $0.49\text{eV}$  which in reasonable agreement with the results reported in  $\text{Eu}^{3+}$  doped other materials<sup>35,36</sup>. These results reflected that the fluorescence temperature quenching was evoked by crossover process.

Figure 4 (a) to (d) show the excitation ( $\lambda_{\text{em}} = 615\text{nm}$ ) and emission ( $\lambda_{\text{ex}} = 328\text{nm}$ ) spectra of well-aligned  $\text{TiO}_2\text{:Sm}$  nanofibres. For the excitation spectra, one intense broad excitation band centred at  $328\text{nm}$  was



**Figure 3.** (a) and (b) are excitation ( $\lambda_{em} = 615$  nm) and emission ( $\lambda_{ex} = 395$  nm) spectra of well-aligned  $\text{TiO}_2$ :Eu fibre arrays with different  $\text{Eu}^{3+}$  dopants calcined at  $500^\circ\text{C}$ , respectively. (c) and (d) are excitation ( $\lambda_{em} = 615$  nm) and emission ( $\lambda_{ex} = 465$  nm) spectra of well-aligned  $\text{TiO}_2$ :1.0 mol% Eu fibre arrays with different calcining temperatures, respectively. (e) Temperature dependence of the relative emission intensity for the  $\text{Eu}^{3+}5\text{D}_0 \rightarrow 7\text{F}_2$  transition in the well-aligned  $\text{TiO}_2$ :1.0 mol% Eu fibre arrays calcined at  $500^\circ\text{C}$ ; the scatter shows experimental data, and the solid lines are fitted functions thereto.

observed, which corresponded to the anatase  $\text{TiO}_2$  host absorption. This evinced an effective energy transfer from the  $\text{TiO}_2$  host to the  $\text{Sm}^{3+}$  ions. Three obvious emission peaks centred at 580, 615, and 660 nm were observed in the emission spectra, which can be ascribed to the transitions from the excited state  ${}^4\text{G}_{5/2}$  to the  ${}^6\text{H}_{5/2}$ ,  ${}^6\text{H}_{7/2}$ , and  ${}^6\text{H}_{9/2}$  states, respectively. As seen from the characteristic peak at 615 nm, the emission intensity decreased with increasing  $\text{Sm}^{3+}$  concentration; however, the emissions of the  $\text{TiO}_2$ :1 mol %  $\text{Sm}^{3+}$  samples, upon increasing the calcining temperature from 500 to  $800^\circ\text{C}$  showed an increasing temperature-dependence (Fig. 4(e)) on the integrated luminescence intensity for the  ${}^4\text{G}_{5/2} \rightarrow {}^6\text{H}_{7/2}$  transition on the  $\text{TiO}_2$ :1 mol %  $\text{Sm}^{3+}$  sample. It can be seen that the integrated emission intensity keeps almost unchanged within the temperature range of 30– $180^\circ\text{C}$ , and then decreases with increasing sample temperature. That is to say, the thermal quenching occurred at temperatures greater than  $180^\circ\text{C}$ . The emission intensity of  $\text{Sm}^{3+}$  decreased to approximately 85% of its low-temperature level at  $400^\circ\text{C}$ . It should also be mentioned that the quenching process, namely the variation trend of integrated



**Figure 4.** (a) and (b) are excitation ( $\lambda_{em} = 615$  nm) and emission ( $\lambda_{ex} = 328$  nm) spectra of well-aligned  $\text{TiO}_2:\text{Sm}^{3+}$  fibre arrays with variable  $\text{Sm}^{3+}$  dopant concentrations calcined at  $600^\circ\text{C}$ , respectively. (c) and (d) are excitation ( $\lambda_{em} = 613$  nm) and emission ( $\lambda_{ex} = 328$  nm) spectra of well-aligned  $\text{TiO}_2:1.0$  mol%  $\text{Sm}$  fibre arrays with different calcining temperatures, respectively. (e) Temperature dependence of the relative emission intensity for  $\text{Sm}^{3+} 4G_{5/2} \rightarrow 6H_{7/2}$  transition in the well-aligned  $\text{TiO}_2:1.0$  mol%  $\text{Sm}$  fibre arrays calcined at  $600^\circ\text{C}$ .

luminescence intensity toward temperature, is extremely different from the one for  $\text{TiO}_2:\text{Eu}^{3+}$ . This is because of the fact that the excited state  $4G_{5/2}$  is much nearer to the neighboring lower state, thus the nonradiative transition can not be omitted at higher temperature. This fact means that the fluorescence temperature quenching can not be simply explained by crossover process.

Figure 5 (a) to (d) show the emission ( $\lambda_{ex} = 328$  nm) spectra of well-aligned  $\text{TiO}_2:\text{Er}$  nanofibres under excitation at 980 nm. The strong, weak, and very weak emission bands located at 550 nm, 525 nm (green region), and 655 nm (red region) were observed, and their intensities monotonically increased with increasing laser working current. The strong 550 nm emission bands, and the weak 525 nm bands in the green region, corresponded to the  $4S_{3/2} \rightarrow 4I_{15/2}$  and  $2H_{11/2} \rightarrow 4I_{15/2}$  transitions, respectively, while the very weak emission 655 nm bands in the red region corresponded to the  $4F_{9/2} \rightarrow 4I_{15/2}$  transition. The green UC emissions were dominant, and the

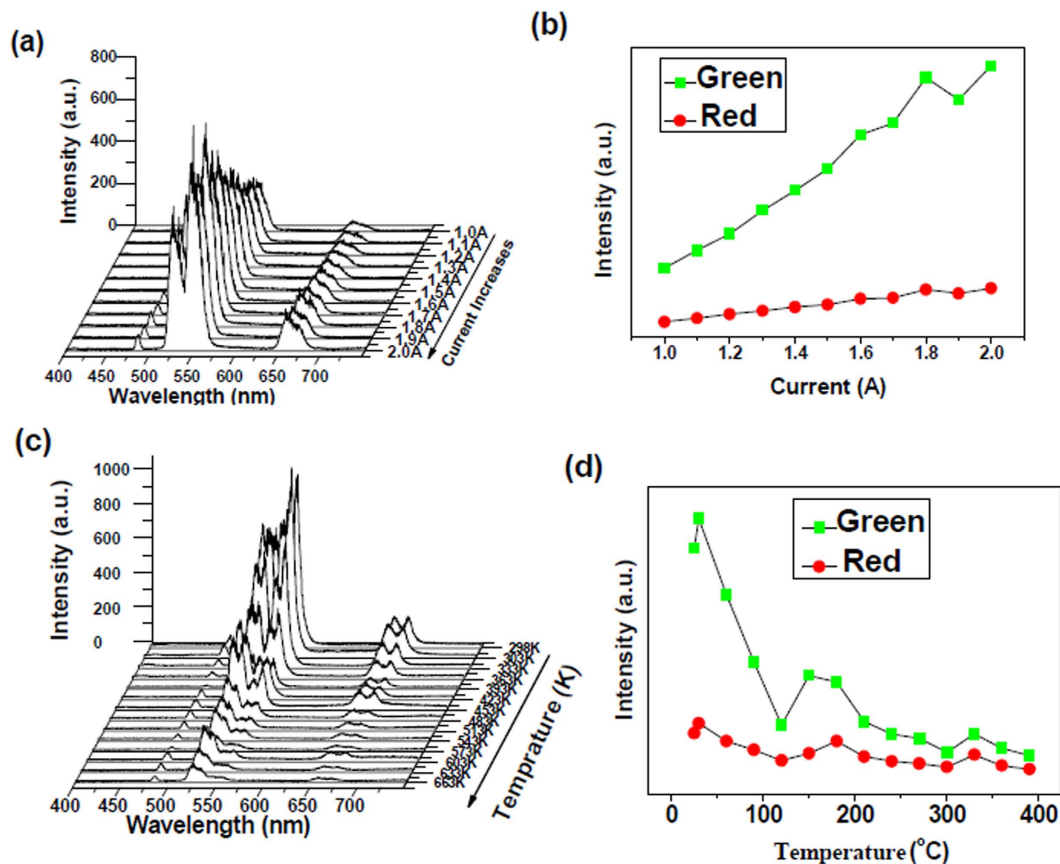


**Figure 5.** (a) Up-conversion emission spectra of  $\text{TiO}_2$ :1.0 mol% Er fibre arrays under excitation at 980 nm; (b) Corresponding dependences of green and red up-conversion emission intensities on the laser working current. (c) Emission spectra of  $\text{TiO}_2$ :1.0 mol% Er fibre arrays measured at various temperatures; (d) Corresponding dependences of green and red up-conversion intensities on sample temperature.

green emission was much more intense than that in the red bandwidth region once the laser working current had been increased; however, the green emission was more rapidly decreased than that in the red region with increasing temperature ( $<120^\circ\text{C}$ ). In comparison with Figs 3(e), 4(e) and 5(d) showed more complicated temperature-dependent fluorescence intensity. Obviously, this temperature of  $\text{Er}^{3+}$  doped  $\text{TiO}_2$  fiber arrays impossible obeys the crossover model since in the UC luminescence process many metastable levels of  $\text{Er}^{3+}$  were involved into the population process, and the populations of all these levels related to the temperature, thus the simple potential barrier model for crossover process can not explain it.

## Conclusions

The continuous, highly oriented,  $\text{TiO}_2$ : $\text{Ln}^{3+}$  ( $\text{Ln} = \text{Eu}, \text{Sm}, \text{or Er}$ ) fibre arrays with linear alignment were successfully prepared by use of an improved electrospinning method. The advantages of the modified method were as follows: (1) exploitation of the viscoelasticity of ultrahigh molecular weight polymer solutions to eliminate the occurrence of bending instability, will lead to a synthetic process that is simple, rapid, efficient, and cost-effective; (2) it can be used to obtain electrospun fibre arrays measuring at least 300 mm in length; (3) the need for a high-speed rotating drum, a manipulating or electrical field, and an expensive collector were all obviated; (4) it provided a continuous fibre-aligning capability and can offer the ability for mass-scale manufacture on a commercial scale. Their luminescence properties were also studied. These results shown that the emission intensity of  $\text{TiO}_2$ : $\text{Eu}^{3+}$  fibre arrays were enhanced with increasing  $\text{Eu}^{3+}$  concentration. On the contrary, the emission intensity of  $\text{TiO}_2$ : $\text{Sm}^{3+}$  fibre arrays decreased with increasing  $\text{Sm}^{3+}$  concentration. The emission intensities of  $\text{TiO}_2$ : $\text{Er}^{3+}$  fibre arrays increased monotonically with increasing laser working current. In addition, these  $\text{TiO}_2$ : $\text{Ln}^{3+}$  fibre arrays presented typical temperature quenching behaviour. Overall, this technique, and its extension to other metal oxides or metal ion-doped oxides, will open up novel routes to the functionalisation of surfaces that can enable the fabrication of new types of optical, electric, magnetic, and tissue engineering devices.

## References

- Jen, H. P., Lin, M. H., Li, L. L., Wu, H. P. & Huang, W. K. High-performance large-scale flexible dye-sensitized solar cells based on anodic  $\text{TiO}_2$  nanotube arrays. *ACS Appl. Mater. & Inter.* **5**, 10098–10104 (2013).
- Liu, S., Hu, J. J., Yan, N. F., Pan, G. L. & Li, G. R. Aluminum storage behavior of anatase  $\text{TiO}_2$  nanotube arrays in aqueous solution for aluminum ion batteries. *Energy & Environ. Sci.* **5**, 9743–9746 (2012).

3. Liu, Z., Zhang, X., Nishimoto, S., Jin, M. & Tryk, D. A. Highly ordered TiO<sub>2</sub> nanotube arrays with controllable length for photoelectrocatalytic degradation of phenol. *J. Phys. Chem. C* **112**, 253–259 (2008).
4. Shao, Z., Zhu, W., Li, Z., Yang, Q. & Wang, G. One-step fabrication of CdS nanoparticle-sensitized TiO<sub>2</sub> nanotube arrays via electrodeposition. *J. Phys. Chem. C* **116**, 2438–2442 (2012).
5. Song, J., Xu, L., Xing, R., Qin, W. & Dai, Q. Ag nanoparticles coated NiO nanowires hierarchical nanocomposites electrode for nonenzymatic glucose biosensing. *Sens. Actuators, B* **182**, 675–681 (2013).
6. Xu, L., Dong, B., Wang, Y., Bai, X. & Liu, Q. Electrospinning preparation and room temperature gas sensing properties of porous In<sub>2</sub>O<sub>3</sub> nanotubes and nanowires. *Sens. Actuators, B* **147**, 531–538 (2010).
7. Qin, W., Xu, L., Song, J., Xing, R. & Song, H. Highly enhanced gas sensing properties of porous SnO<sub>2</sub>-CeO<sub>2</sub> composite nanofibers prepared by electrospinning. *Sens. Actuators, B* **185**, 231–237 (2013).
8. Zhou, C., Xu, L., Song, J., Xing, R. & Xu, S. Ultrasensitive non-enzymatic glucose sensor based on three-dimensional network of ZnO-CuO hierarchical nanocomposites by electrospinning. *Sci. Rep-UK* **4**, 7382 (2014).
9. Xing, R., Xu, L., Song, J., Zhou, C. & Li, Q. Preparation and gas sensing properties of In<sub>2</sub>O<sub>3</sub>/Au nanorods for detection of volatile organic compounds in exhaled breath. *Sci. Rep-UK* **5**, 10717 (2015).
10. Paulose, M., Shankar, K., Yoriya, S., Prakasam, H. E. & Varghese, O. K. Anodic growth of highly ordered TiO<sub>2</sub> nanotube arrays to 134 μm in length. *J. Phys. Chem. B* **110**(33), 16179–16184 (2006).
11. Zhou, H. & Zhang, Y. Electrochemically self-doped TiO<sub>2</sub> nanotube arrays for supercapacitors. *J. Phys. Chem. C* **118**, 5626–5636 (2014).
12. Yu, Z., Qu, X., Yang, W., Peng, J. & Xu, Z. Hydrothermal synthesis and memristive switching behaviors of single-crystalline anatase TiO<sub>2</sub> nanowire arrays. *J. Alloy. Compd.* **15**, 294–300 (2016).
13. Dersch, R., Liu, T., Schaper, A. K., Greiner, A. & Wendorff, J. H. Electrospun nanofibers: Internal structure and intrinsic orientation. *J. Polym. Sci. Part B* **41**, 545–553 (2003).
14. Liu, Z., Li, X., Yang, Y., Zhang, K. & Wang, X. Control of structure and morphology of highly aligned PLLA ultrafine fibers via linear-jet electrospinning. *Polymer* **54**, 6045–6051 (2013).
15. Zhou, Q., Bao, M., Yuan, H., Zhao, S. & Dong, W. Implication of stable jet length in electrospinning for collecting well-aligned ultrafine PLLA fibers. *Polymer* **54**, 6867–6876 (2013).
16. Theron, A., Zussman, E. & Yarin, A. L. Formation of nanofiber crossbars in electrospinning. *Appl. Phys. Lett.* **82**, 973 (2003).
17. Theron, A., Zussman, E. & Yarin, A. L. Electrostatic field-assisted alignment of electrospun nanofibres. *Nanotechnology* **12**, 3–7 (2001).
18. Li, D. & Xia, Y. Electrostatic field-assisted alignment of electrospun nanofibres. *Nano. Lett.* **3**, 555–560 (2003).
19. Xu, S., Dong, B., Zhou, D., Yin, Z. & Cui, S. Paper-based upconversion fluorescence resonance energy transfer biosensor for sensitive detection of multiple cancer biomarkers. *Sci. Rep-UK* **6**, 23406 (2016).
20. Dong, B., Liu, D. P., Wang, X. J., Yang, T. & Miao, S. M. Optical thermometry through infrared excited green upconversion emissions in Er<sup>3+</sup>-Yb<sup>3+</sup> codoped Al<sub>2</sub>O<sub>3</sub>. *Appl. Phys. Lett.* **90**, 181117 (2007).
21. Dong, B., Hua, R. N., Cao, B. S., Li, Z. P. & He, Y. Y. Size dependence of the upconverted luminescence of NaYF<sub>4</sub>:Er,Yb microspheres for use in ratiometric thermometry. *Phys. Chem. Chem. Phys.* **16**, 20009–20012 (2014).
22. Dong, B., Cao, B., He, Y., Liu, Z. & Li, Z. Temperature sensing and *in vivo* imaging by molybdenum sensitized visible upconversion luminescence of rare-earth oxides. *Adv. Mater.* **24**, 1987–1993 (2012).
23. Liu, K., Zhang, Z., Shan, C., Feng, Z. & Li, J. A flexible and superhydrophobic upconversion luminescence membrane as an ultrasensitive fluorescence sensor for single droplet detection. *Light-Sci. Appl.* **5**, e16136 (2016).
24. Yu, H., Li, T., Chen, B., Wu, Y. & Li, Y. Preparation of aligned Eu(DBM)phen/PS fibers by electrospinning and their luminescence properties. *J. Colloid. Interf. Sci.* **400**, 175–180 (2013).
25. Huang, Z., Zhang, Y. Z., Kotaki, M. & Ramakrishn, S. A review on polymer nanofibers by electrospinning and their applications in nanocomposites. *Compos. Sci. Technol.* **63**, 2223–2253 (2003).
26. Luo, G., Teh, K. S., Liu, Y., Zang, X. & Wen, Z. Direct-write, self-aligned electrospinning on paper for controllable fabrication of three-dimensional structures. *ACS Appl. Mater. Inter.* **7**, 27765–27770 (2015).
27. Valente, T. A., Silva, D. M., Gomes, P. S., Fernandes, M. H. & Santos, J. D. Effect of sterilization methods on electrospun poly(lactic acid) (PLA) fiber alignment for biomedical applications. *ACS Appl. Mater. Inter.* **8**, 3241–3249 (2016).
28. Chew, S. Y., Mi, R., Hoke, A. & Leong, K. W. The effect of the alignment of electrospun fibrous scaffolds on Schwann cell maturation. *Biomaterials* **29**, 653–661 (2008).
29. Dong, G., Xiao, X., Chi, Y., Qian, B. & Liu, X. Polarized luminescence properties of TiO<sub>2</sub>:Sm<sup>3+</sup> microfibers and microbelts prepared by electrospinning. *J. Phys. Chem. C* **113**, 9595–9600 (2009).
30. Yi, S., Bae, J. S., Moon, B. K., Jeong, J. H. & Kim, J. H. Highly enhanced luminescence of nanocrystalline TiO<sub>2</sub>:Eu<sup>3+</sup> phosphors. *Opt. Mater.* **28**, 610–614 (2006).
31. Leostean, C., Stefan, M., Pana, O., Cadis, A. I. & Suci, R. C. Properties of Eu doped TiO<sub>2</sub> nanoparticles prepared by using organic additives. *J. Alloy. Compd.* **575**, 29–39 (2013).
32. Tian, Y., Chen, B. J., Hua, R. N., Sun, J. S. & Cheng, L. H. Optical transition, electron-phonon coupling and fluorescent quenching of La<sub>2</sub>(MoO<sub>4</sub>)<sub>3</sub>:Eu<sup>3+</sup> phosphor. *J. Appl. Phys.* **109**, 053511 (2011).
33. Van Uitert, L. G. Characterization of energy transfer interactions between rare earth ions. *J. Electrochem. Soc.* **114**, 1048–1053 (1967).
34. Struck, C. W. & Fonger, W. H. Quantum-mechanical treatment of Eu<sup>3+</sup> 4f → 4f and 4f? charge-transfer-state transitions in Y<sub>2</sub>O<sub>3</sub> and La<sub>2</sub>O<sub>3</sub>. *J. Chem. Phys.* **64**, 1784–1790 (1976).
35. Tian, B., Chen, B., Tian, Y., Li, X. & Zhang, J. Excitation pathway and temperature dependent luminescence in color tunable Ba<sub>2</sub>Gd<sub>8</sub>Zn<sub>4</sub>O<sub>21</sub>:Eu<sup>3+</sup> phosphors. *J. Mater. Chem. C* **1**, 2338–2344 (2013).
36. Tian, Y., Chen, B., Hua, R., Yu, N. & Liu, B. Self-assembled 3D flower-shaped NaY(WO<sub>4</sub>)<sub>2</sub>:Eu<sup>3+</sup> microarchitectures: Microwave-assisted hydrothermal synthesis, growth mechanism and luminescence properties. *CrystEngComm* **14**, 1760–1769 (2012).

## Acknowledgements

The authors thank, for their financial support: the Programme for Liaoning Excellent Talents in the University (Grant no. LJQ2011047), the Programme for Liaoning BaiQianWan Talents (Grant no. 2014921063), the Natural Science Foundation of Liaoning Province (Grant no. 2013023034), the Dalian Municipal Science and Technology Plan Project (Grant no. 2014E14SF179), the Liaoning Natural Science Foundation of China (Grant no. 2015020203), and National Training Programmes for Innovation and Entrepreneurship for Undergraduates (No. 201510150019).

## Author Contributions

Yue Li, Yang Song, Yanning Tang and Shimin Liu managed the long-term experiments and processed the data. Hongquan Yu, Yanbo Wu and Baojiu Chen wrote the main manuscript. All other authors contributed to the discussion and revision of the content.



## Additional Information

**Supplementary information** accompanies this paper at <http://www.nature.com/srep>

**Competing Interests:** The authors declare no competing financial interests.

**How to cite this article:** Yu, H. *et al.* Ultralong well-aligned  $\text{TiO}_2\text{:Ln}^{3+}$  (Ln = Eu, Sm, or Er) fibres prepared by modified electrospinning and their temperature-dependent luminescence. *Sci. Rep.* 7, 44099; doi: 10.1038/srep44099 (2017).

**Publisher's note:** Springer Nature remains neutral with regard to jurisdictional claims in published maps and institutional affiliations.



This work is licensed under a Creative Commons Attribution 4.0 International License. The images or other third party material in this article are included in the article's Creative Commons license, unless indicated otherwise in the credit line; if the material is not included under the Creative Commons license, users will need to obtain permission from the license holder to reproduce the material. To view a copy of this license, visit <http://creativecommons.org/licenses/by/4.0/>

© The Author(s) 2017